SCIENTIFIC REPORTS

OPEN

SUBJECT AREAS:

SUPERCONDUCTING DEVICES

SUPERCONDUCTING PROPERTIES AND MATERIALS

PHASE TRANSITIONS AND CRITICAL PHENOMENA

Received
3 February 2014

Accepted
6 June 2014

Published
25 June 2014

Correspondence and requests for materials should be addressed to C.-T.L. (ctliang@phys.ntu.edu.tw)

* These authors contributed equally to this work.

Spin-orbit-coupled superconductivity

Shun-Tsung Lo[1]*, Shih-Wei Lin[2]*, Yi-Ting Wang[3], Sheng-Di Lin[2] & C.-T. Liang[1,3]

[1]Graduate Institute of Applied Physics, National Taiwan University, Taipei 106, Taiwan, [2]Department of Electronics Engineering, National Chiao Tung University, Hsinchu 300, Taiwan, [3]Department of Physics, National Taiwan University, Taipei 106, Taiwan.

Superconductivity and spin-orbit (SO) interaction have been two separate emerging fields until very recently that the correlation between them seemed to be observed. However, previous experiments concerning SO coupling are performed far beyond the superconducting state and thus a direct demonstration of how SO coupling affects superconductivity remains elusive. Here we investigate the SO coupling in the critical region of superconducting transition on Al nanofilms, in which the strength of disorder and spin relaxation by SO coupling are changed by varying the film thickness. At temperatures T sufficiently above the superconducting critical temperature T_c, clear signature of SO coupling reveals itself in showing a magneto-resistivity peak. When $T < T_c$, the resistivity peak can still be observed; however, its line-shape is now affected by the onset of the quasi two-dimensional superconductivity. By studying such magneto-resistivity peaks under different strength of spin relaxation, we highlight the important effects of SO interaction on superconductivity.

Spin-orbit (SO) interaction, which couples the electron orbital motion to its spin, has been at the center of intensive research efforts in the field of spintronics[1–3]. This coupling between orbital motion and spin orientation leads to several interesting physical phenomena such as the spin Hall effects[4,5], spin-orbit gap[6,7] and spin relaxation[8,9], and may open an avenue to achieve all-electrical control of spin degree of freedom[10]. In addition, SO interaction provides an essential ingredient in creating topological insulators[11] and Majorana fermions[12]. Furthermore, recently SO coupling was found to have a significant impact on quasi two-dimensional (2D) superconductivity. One of the most fascinating examples is the promotion of superconductivity with enhancing the strength of SO interaction[13]. In the 2D electron gas at the interface between $LaAlO_3$ and $SrTiO_3$ exhibiting superconducting properties at low temperatures T, large Rashba SO coupling arising from interfacial breaking of inversion symmetry is shown to have pronounced effects in stabilizing the superconducting state[13,14]. Moreover, due to strong SO coupling at the interface, ferromagnetism, which is usually thought to be incompatible with conventional superconductivity, can now coexist with superconductivity[15,16]. Interestingly, SO coupling also appears relevant to the observed increase of superconducting critical temperature T_c by an in-plane magnetic field in Pb thin films[17]. Within the framework of the Bardeen-Cooper-Schrieffer (BCS) theory[18] which attributes superconductivity to pairs of electrons with opposite spin projections (Cooper pairs), any mechanism that causes spin alignment (like those induced by paramagnetic impurities and magnetic fields) is not predicted to enhance superconductivity. Response of superconductivity to magnetic perturbations can be fundamentally different in the presence of SO coupling.

In a quasi 2D superconductor with SO coupling, the application of a magnetic field perpendicular to the plane of carrier motion may not only lead to suppression of weak antilocalization (WAL) induced by SO coupling[19–24], but also to orbit de-pairing of Cooper pairs, destroying the zero-resistivity superconducting state. Magneto-transport studies could thereby allow one to obtain fundamental information regarding the interplay between SO coupling and superconductivity. Here we present such measurements on molecular-beam epitaxy (MBE)-grown Al nanofilms with thicknesses of 3 nm, 6 nm, and 12 nm in which the rate of spin relaxation by SO coupling depends on the nanofilm thickness. To date, most measurements concerning SO coupling are performed far beyond the superconducting state, making a direct demonstration of how SO coupling affects superconductivity unavailable. In our experiments, when $T \gg T_c$, a WAL peak in the magneto-resistivity due to the presence of SO coupling is observed in all the nanofilms. By probing the temperature evolution of this resistivity peak toward the superconducting state, we have demonstrated that WAL effects are progressively suppressed as a result of the onset of superconductivity. In the superconducting state, the peak shape is clearly affected by Cooper paring. Moreover, an unusual positive contribution to the magneto-resistivity (unexpected within the BCS theory and WAL effects) appears near the resistivity peak for the 3-nm-thick Al film in which the relaxation of spin is fastest among the three studied films. Our experimental work therefore highlights the important effects of SO coupling on superconductivity.

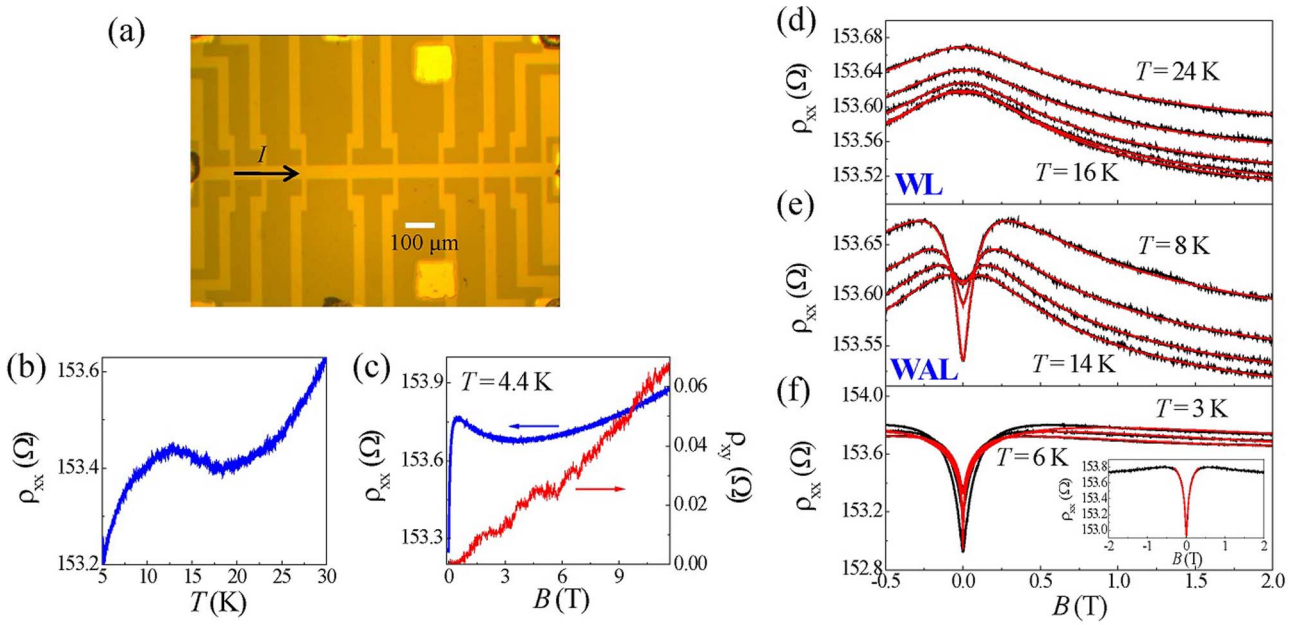

Figure 1 | (a) Optical image of the 6-nm-thick Al film. (b) Longitudinal resistivity ρ_{xx} as a function of T. (c) Longitudinal and Hall resistivities ρ_{xx} and ρ_{xy} as a function of B up to 11.7 T at $T = 4.4$ K. $\rho_{xx}(B)$ at various T. From top to bottom at $B = 2$ T: (d) $T = 24$ K, 22 K, 20 K, 18 K, and 16 K; (e) $T = 8$ K, 10 K, 12 K, and 14 K; (f) $T = 3$ K, 4 K, and 6 K. The red curves correspond to the best fits to Eq. (1). The inset of (f) presents the fit considering Maki-Thompson superconducting fluctuations to the data at $T = 3$ K.

Results

SO coupling in the normal state. Figure 1(a) shows the optical image of the studied 6-nm-thick device and Fig. 1(b) shows the obtained longitudinal resistivity ρ_{xx} over a wide range of temperature (5 K $\leq T \leq$ 30 K). For $T >$ 18 K, ρ_{xx} increases with increasing T, characteristics of a metal film subject to electron-phonon scattering. For $T <$ 18 K, quantum corrections primarily due to WAL and superconducting fluctuations would then instead govern the T dependence of resistivity as the effects of electron-phonon scattering is suppressed. Figure 1(c) shows the magneto-resistivity measurements for $0 < B <$ 11.7 T at $T = 4.4$ K. We can observe that ρ_{xx} is much larger than the Hall resistivity ρ_{xy} over the whole field range. The smallness of ρ_{xy} is due to a large carrier density in metal systems. Therefore one is able to obtain the longitudinal conductivity of $\sigma_{xx} \approx 1/\rho_{xx}$ according to $\sigma_{xx} = \rho_{xx}/(\rho_{xx}^2 + \rho_{xy}^2)$.

Figures 1(d)–(f) show $\rho_{xx}(B)$ at various T. As presented in Fig. 1(e), for 8 K $\leq T \leq$ 14 K, signatures of WAL effects, that is, positive magneto-resistivity (MR) around $B = 0$ followed by negative MR with increasing B, are observed, clearly indicating the importance of SO coupling in the measured Al nanofilm with thickness of $d =$ 6 nm. For $T \geq$ 16 K, weak localization (WL) instead of WAL dominates the transport process, inferred from the monotonically decreasing trend of ρ_{xx} with the applied B shown in Fig. 1(d). Suppression of WAL at elevated T is expected to occur when no significant spin-dependent phases can be accumulated. In metals, the dominant mechanism of SO coupling is believed to arise from the potential of lattice ions such that the spin orientation is randomized following the Elliot-Yafet (EY) mechanism which states that spin flips during every scattering event[2,19,25]. According to the WAL theory developed by Hikami, Larkin, and Nagaoka (HLN) (ref. 26), which assumes that the EY mechanism is responsible for spin relaxation, the MR in the 2D diffusive regime under $\sigma_{xx} \approx 1/\rho_{xx}$ has the form

$$\frac{1}{\rho_{xx}} = \sigma_{xx}^0 + \frac{e^2}{2\pi^2\hbar} \left\{ \frac{3}{2}\Psi\left(\frac{1}{2}+\frac{B_2}{B}\right) - \Psi\left(\frac{1}{2}+\frac{B_1}{B}\right) - \frac{1}{2}\Psi\left(\frac{1}{2}+\frac{B_3}{B}\right) - \ln\left(\frac{B_2^{3/2}}{B_1 B_3^{1/2}}\right) \right\}, \quad (1)$$

where σ_{xx}^0 is the zero-field conductivity independent of B, $\Psi(x)$ is the digamma function, $B_1 = B_0 + B_{SO}$, $B_2 = B_\phi + \frac{4}{3}(B_{SO})$, and $B_3 = B_\phi$. Here the characteristic fields B_0, B_{SO} and B_ϕ are related to the elastic scattering length l_0, spin-orbit relaxation length l_{SO}, and dephasing length l_ϕ through $B_0 = \frac{\hbar}{2el_0^2}$, $B_{SO} = \frac{\hbar}{4el_{SO}^2}$ and $B_\phi = \frac{\hbar}{4el_\phi^2}$. The red curves in Figs. 1(d)–(f) denote the best fits to the data using Eq. (1). The excellent agreement between experiments and HLN theory shown in Figs. 1(d) and 1(e) for 8 K $\leq T \leq$ 24 K suggests that the EY process is indeed the dominant mechanism for spin relaxation. However, it is found in Fig. 1(f) that HLN theory fails to describe the MR behavior for $T <$ 6 K, which is ascribed to the influence of fluctuating Cooper pairing (superconducting fluctuations). The inset of Fig. 1(f) presents the fitting result considering SO interaction and Maki-Thompson superconducting fluctuations. A good agreement can likewise be observed. However such a method is not applicable as the superconducting state is well developed.

SO coupling in the superconducting state. In order to study the interplay between SO coupling and superconducting fluctuations around $B = 0$, we limit the fitting range to high magnetic fields, in which superconductivity is completely suppressed, to obtain the SO relaxation and dephasing length. Here we choose the field B_p at which $\rho_{xx}(B)$ reaches its maximum as the lower bound to fit our data to Eq. (1). The underlying reason for this choice is that superconductivity *cannot* give rise to negative MR. On the other hand, the upper limit of this fit is chosen at $B = 2$ T to avoid the influence of positive MR which occurs at high fields due to orbital motion as shown in Fig. 1(c). The new fits to the data are shown as the red curves in Fig. 2(a) for 3 K $\leq T \leq$ 6 K and further in Fig. 2(b) for 0.328 K $\leq T \leq$ 1.980 K, where remarkable agreement between theory and experiments is found. Three important length scales l_0, l_{SO}, and l_ϕ can thereby be determined and the results are plotted against T in Figs. 3(a) and 3(b). We observe that l_{SO} exceeds l_ϕ for $T \geq$ 14 K, indicating that phase coherence has lost before spin-dependent phase is accumulated for $T \geq$ 14 K. Consistently, WAL effects are barely observable for $T >$ 14 K in Fig. 1(d). As shown in

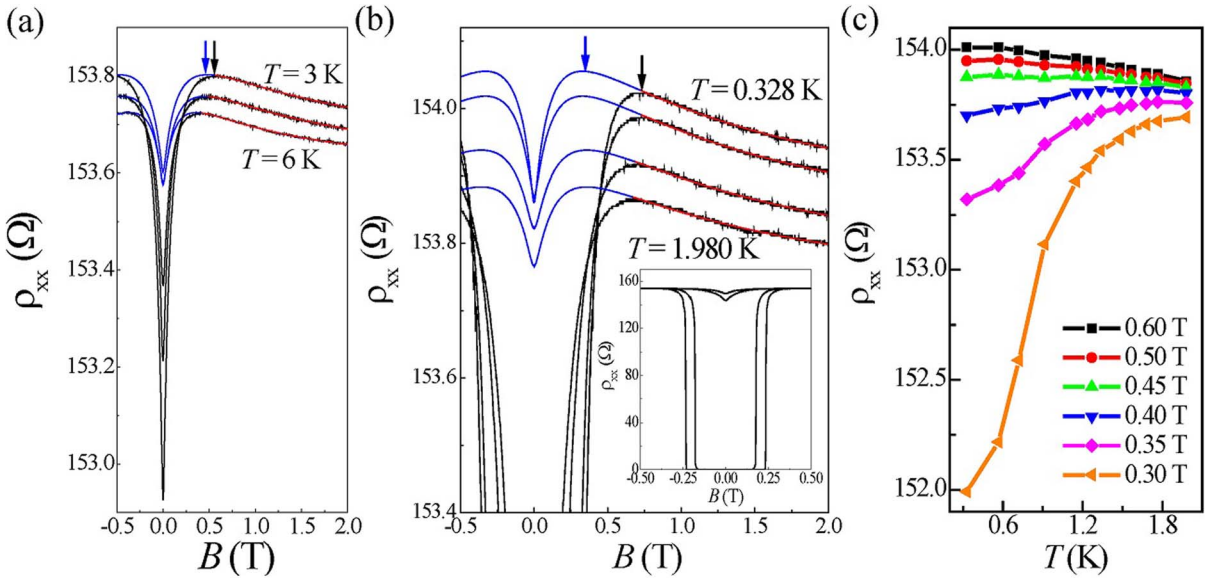

Figure 2 | $\rho_{xx}(B)$ at selected temperatures T for the 6-nm-thick film. From top to bottom at $B = 2$ T: (a) $T = 3$ K, 4 K, and 6 K; (b) $T = 0.328$ K, 0.914 K, 1.568 K, and 1.980 K. The red curves represent the best fits to Eq. (1) over the limited field range ($B_p \leq B \leq 2$ T) and the blue curves denote the extrapolations of the fits to low B regime using the extracted parameters. The black and blue arrows indicate the experimentally obtained and theoretically predicted peak positions. To emphasize the zero-resistivity superconducting state around $B = 0$ when $T \leq 1.980$ K, the full-scale view at the corresponding T are shown in the inset of (b). (c) $\rho_{xx}(T)$ at various B around the superconducting transition.

the inset of Fig. 2(b), the zero-resistivity superconducting state appears when T is low enough. The characterization of the 6-nm-thick superconducting nanofilm which yields important physical quantities can be found in the supplementary information. To further study the effects of Cooper pairing, we plot the theoretical curves given by Eq. (1) around $B = 0$ with the parameters determined from the fitting procedure at high B as described above. These simulation curves, which are the extrapolation of the fitting curves, are represented by the blue ones in Fig. 2(a). The expected influence of superconductivity on WAL can then be tracked as a function of T even down to 0.328 K, well inside the superconducting regime. By plotting $\rho_{xx}(T)$ at different B in Fig. 2(c), we observe that there is a crossover between superconducting and insulating states with B.

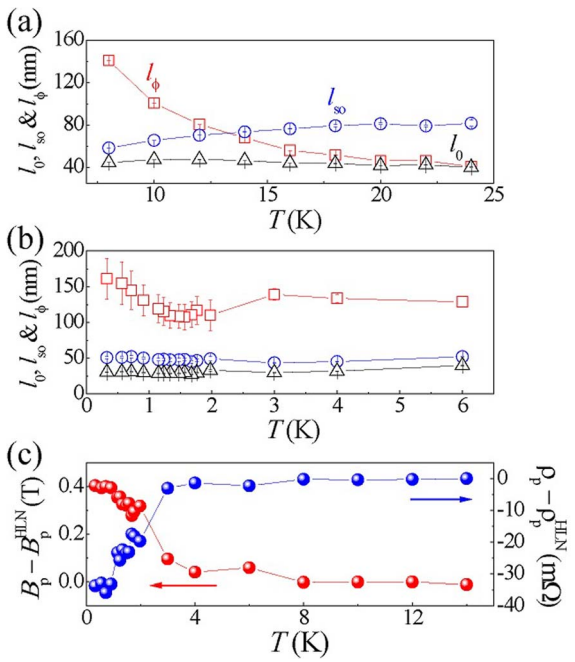

Figure 3 | Dephasing length l_ϕ, spin-orbit relaxation length l_{SO}, and elastic scattering length l_0 as a function of T ranging from (a) 8 K to 24 K and (b) from 0.328 to 6 K. (c) The difference between the measured and theoretically predicted resistivity peak position (ρ_p and ρ_p^{HLN} at $B = B_p$ and B_p^{HLN}, respectively) as a function of T.

By comparing the experimental data (where both SO and superconductivity exist) with the simulated curves (where only SO is considered) as shown in Figs 2(a) and 2(b), we observe that the position of resistivity peak, characterized by strong SO coupling in the normal state, is shifted to a higher magnetic field compared with the expected position when $T \leq 6$ K. Figure 3(c) then collects the difference between the measured and theoretical peak positions in their resistivity and magnetic field values at various T covering both the normal and superconducting states. This difference becomes significant at low T, suggestive of suppression of WAL effects by spin-singlet Cooper pairing. In the normal state, positive MR around $B = 0$ is due to SO coupling. In contrast, in the superconducting state, orbit de-pairing by magnetic field, leading to notable positive MR, plays a decisive role in the low-field magneto-transport properties since SO coupling has limited effects on carriers with total spin zero such as bosons. However, in the transition regime from normal to superconducting state, the orbital motion of spin-half electrons, which are fermions, still couples to their spin orientations due to SO interaction.

As shown in Fig. 2 (b), in the normal state indicated by the red fitted curves, ρ_{xx} decreases with increasing temperature, characteristic of a weak insulator. When B is below B_p, positive magnetoresistivity is observed and insulating behavior persists before the resistivity of the device reduces dramatically due to superconductivity. Since the ρ_{xx} maxima predicted by the standard HLN model (indicated by the blue curves) occur at a substantially lower B than those observed in experiments, ρ_{xx} for $B < B_p$ cannot be solely described by spin-orbit coupling in the normal state and thus must be related to superconductivity. Such results are reminiscent of the intriguing influence of disorder on superconductivity[27–33]. In a disordered superconductor subject to a strong perpendicular magnetic field, insulating behavior can occur. For a moderate amount of disorder in the system, the observed insulating behavior at high fields is

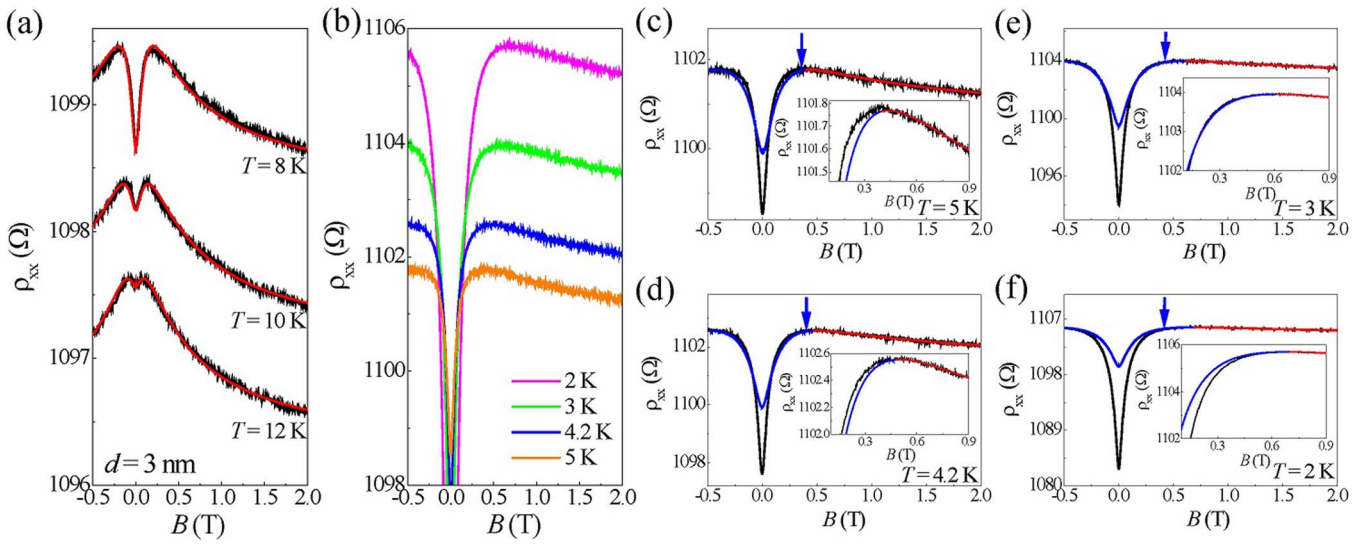

Figure 4 | (a) & (b) Magneto-resistivity measurements $\rho_{xx}(B)$ at different temperatures T for the 3-nm-thick film. The red curves correspond to the best fits to Eq. (1). (c) – (f) Zoom-in of (b) at each separate T. The insets show $\rho_{xx}(B)$ around B_p indicated by the arrows. The red curves are the best fits to Eq. (1) over the limited field range ($B_p \leq B \leq 2$ T) and the blue curves denote the extrapolations of the fits to low B regime using the extracted parameters.

generally ascribed to localization of unpaired electrons. However, in a strongly disordered superconductor, increasing magnetic field does not always quench superconductivity[34–36]. Instead, thanks to the formation of superconducting islands (SCIs), with the presence of strong disorder, an applied out-of-plane magnetic field, which suppresses the correlations between different superconducting islands, is not detrimental to superconductivity drastically. The route toward insulating behavior with increasing magnetic field thereby proceeds through development of well-separated superconducting islands followed by localization of unpaired electrons, which is unexpected within the conventional BCS theory. Such an unusual superconductor-insulator transition (SIT) has already been observed in a wide variety of amorphous superconducting thin films including In_xO_y (ref. 27), TiN (ref. 29), and Bi (ref. 31). Strong disorder, which is believed to be detrimental to superconductivity, plays a crucial role in maintaining superconductivity in such systems. In the presence of strong disorder, normal-state transport should be governed by activation or hopping process, giving rise to an exponential T dependence of resistivity[27,30,31,37]. In our MBE-grown nanofilms, disorder may not be strong enough to support the formation of SCIs, which can be understood from the observed weak T dependence of ρ_{xx} at $B = 2$ T shown in Fig. 2(b). Moreover, the obtained ρ_{xx} over the whole measurement range is far below $\frac{h}{2e^2} \approx 13$ kΩ which is the critical resistivity value expected for the onset of strong localization.

Further magneto-transport measurements were performed on the Al nanofilms with thickness of 3 nm and 12 nm, which are expected to have respectively faster and slower spin relaxation compared with that of 6 nm. Figures 4(a) and 4(b) show the measured $\rho_{xx}(B)$ at various T for the 3-nm-thick film. We observe that positive MR around $B = 0$ due to WAL, can be well fitted to Eq. (1) for $T \geq 8$ K. For $T < 8$ K, influence of superconductivity on the magneto-resistivity becomes increasingly important with decreasing T. For clarity, we plot $\rho_{xx}(B)$ at $T = 5$ K, 4.2 K, 3 K, and 2 K separately in Figs. 4(c)–(f). The experimental data are in good agreement with WAL theory described by Eq. (1) when $B > B_p$, the field where the resistivity peak occurs. Following the same analysis procedure done for the 6-nm-thick film, we extrapolate the high-field fitting curves to lower fields by directly substituting the extracted fitting parameters into Eq. (1). Interestingly, as seen by the comparison between measured and simulated curves for $B < B_p$, superconductivity does not always cause the measured resistivity to be *lower* than that predicted by Eq. (1) for a given B. For example, figure 5(c) shows that at $T = 5$ K the magneto-resistivity near B_p is higher than its expected value without taking superconducting effects into account given by Eq. (1). With decreasing T, this unusual positive resistivity contribution becomes gradually smaller and eventually disappears, which is observed clearly in the insets of Figs. 4(c) – (f), the zoom-in of the region around B_p. At lower T and B, the resistivity value is always lower than the prediction of Eq. (1) due to stronger Cooper-pair correlations. Such results indicate that there will be a mechanism relevant to Cooper pairing which makes the resistivity higher than that predicted by Eq. (1).

The enlargement of SCI size with decreasing B is thought to be one of the mechanism which can provide an extra resistivity contribution. With a decrease in B, the enlarged SCIs may further block the electron transport. As observed in Fig. 4(b), even for the 3-nm-thick film, the T dependence of ρ_{xx} around B_p is still very weak and $\rho_{xx}(B) \ll \frac{h}{2e^2} \approx 13$ kΩ, suggesting that disorder does not play a key role in our observed resistivity anomaly. It is noted that the magneto-transport measurements followed by the same analysis procedures have also been done for $T < 2$ K. All of them share the same features with that at $T = 2$ K shown in Fig. 4(f), where Cooper pairing appears to cause the measured resistivity to be lower than that predicted by Eq. (1) over the whole B range below B_p. At $T < 2$ K, since superconducting correlations are strong, this unusual resistivity contribution is completely suppressed. Finally figures 5(a) and 5(b) show the magneto-transport data measured on the 12-nm-thick film. The resistivity peak well described by Eq. (1) in the normal state is completely suppressed at low temperatures. In the 12-nm-thick film, strong superconducting correlation completely suppresses the influence of SO coupling.

Discussion

The physical quantities of superconductivity and SO coupling obtained from the fits for the Al nanofilms of various thicknesses are summarized in Table 1. We note that ξ is longer than the film thickness in all our samples. Therefore we always have quasi-2D superconductivity. We can clearly see in Table 1 that τ_{SO} ($= l_{SO}^2/D$) (ref. 38) decreases with decreasing the film thickness, indicating

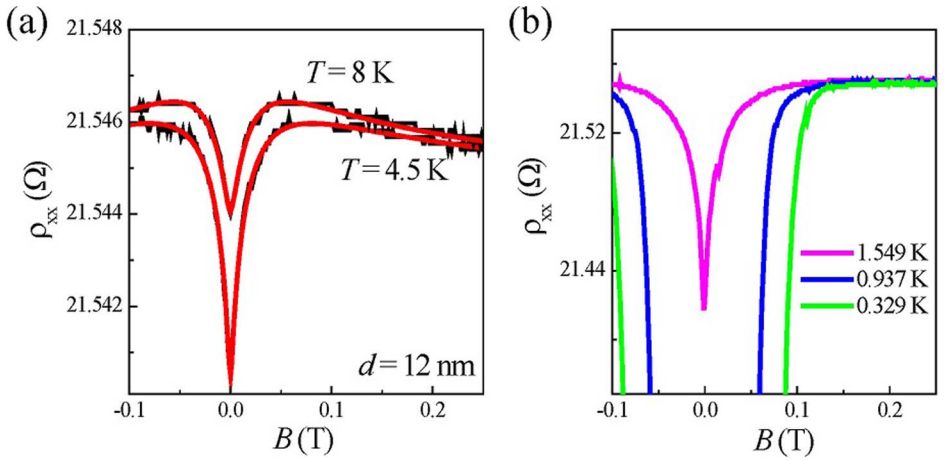

Figure 5 | (a) & (b) Magneto-resistivity measurements $\rho_{xx}(B)$ on the 12-nm-thick film at different temperatures T. The red curves correspond to the best fits to Eq. (1).

that the strength of spin relaxation is stronger in a thinner film. Correspondingly, the amount of disorder increases with decreasing the film thickness, which can be understood from the comparison of the zero-field resistivity at $T = 8$ K well above T_c and from the temperature dependence of resistivity $\rho(T, B = 0)$ for $T \geq 8$ K (see the Supplementary Fig. S1). We can see clearly that the insulating behavior becomes progressively stronger with reducing the film thickness. It is known that two extensively studied effects of spin relaxation are the Elliot-Yafet and Dyakonov-Perel (DP) mechanisms[2,25,39,40]. In the EY mechanism, spin relaxation is relevant to how the spin changes its orientation during a scattering process. This is possible as the electron wave functions associated with a given spin acquire an admixture of the opposite-spin state due to SO coupling induced by lattice ions. In contrast, the DP mechanism is related to the Dresselhaus SO coupling caused by bulk inversion asymmetry and the Rashba SO coupling caused by structural inversion asymmetry. In this case, a charged particle moving in an electric field (originating from the lack of inversion symmetry) experiences an effective magnetic field, which couples to its spin. The spin relaxation is thereby relevant to spin precession around this effective magnetic field between scattering events. Therefore, increasing disorder may enhance the rate of spin relaxation govern by EY mechanism. Moreover, as shown in the Supplementary Fig. S2, the model developed by Iordanskii, Lyanda-Geller and Pikus (ILP) (ref. 41), in which the DP mechanism is included, cannot yield good fits to the measured MR data as compared to the HLN model especially in the 3-nm-thick film with the strongest disorder in our experiments. These results indicate that EY mechanism dominates over DP one with decreasing the nanofilm thickness.

The scale of energy variation involved due to spin relaxation can be evaluated utilizing the uncertainty relation $\varepsilon_{SO} = h/\tau_{SO}$ (ref. 14). By calculating the ratio of ε_{SO} to 2Δ, which is found to be 0.37, 0.77, and 0.85 for the films of $d = 12$ nm, 6 nm, and 3 nm, respectively, the growing importance in the correlation between spin relaxation and superconductivity with decreasing the film thickness is thereby revealed. Correspondingly, l_{SO} approaches progressively to ξ. This numerical analysis suggests that the unexpected resistivity contribution around B_p observed in the 3-nm-thick film is indeed related to the combination effects of SO coupling which causes spin relaxation and superconductivity which pairs electron spins. It is well-established that the incoming electron with spin-up takes another electron with spin-down to enter the BCS superconductor as a Cooper pair with zero spin. The attractive interaction that pairs the electrons to form superconducting state can be mediated by lattice vibrations as described by the BCS theory. Since the SO coupling involved here is provided by the potential of charged atoms, in a material preserving ideal crystalline structure, spin orientation relaxes spatially homogeneously. However, in the presence of disorder this process will then become inhomogeneous. Our experimental findings thus provide an systematic way to probe the influence of SO coupling on superconductivity by studying the evolution of magneto-resistivity peak in the superconducting state.

In conclusion, magneto-transport in the Al nanofilms of different thicknesses (3 nm, 6 nm, and 12 nm) was investigated using weak antilocalization analysis. For all the films in the normal state, we observe clear signatures of WAL, that is, positive magneto-resistivity around $B = 0$ followed by negative one with increasing B, indicating the importance of spin-orbit coupling. Moreover, all the measured MR in the normal state agrees well with the calculation work done by Hikami, Larkin, and Nagaoka. With decreasing temperature, which causes the onset of superconductivity, we show that the MR peak due to SO coupling in the normal state would now be govern by the interplay of SO coupling and superconductivity. For the 6-nm-thick film, Cooper pairing reduces the resistivity from the value predicted by HLN theory and thereby shifts the MR peak to a higher B. More interestingly, we find that there is an extra resistivity contribution

Table 1 | Summary of the physical quantities of superconductivity and spin-orbit coupling

	Superconductivity					Spin-orbit interaction			Disorder strength	Coupling strength	
d	T_c	2Δ	$H_c(0)$	ξ	D	l_{so}[a]	τ_{SO}	ε_{SO}	$\rho_{xx}(T = 8\ K, B = 0)$		
nm	K	meV	T	nm	10^{-4} m^2/s	nm	10^{-11} sec	meV	Ω	$\varepsilon_{so}/2\Delta$	l_{so}/ξ
3	1.509	0.46	0.339	31.18	2.44	51.30	1.08	0.39	1099	0.85	1.65
6	1.577	0.48	0.424	27.88	2.04	48.12	1.13	0.37	154	0.77	1.73
12	1.358	0.41	0.139	48.69	5.36	120.90	2.72	0.15	22	0.37	2.48

[a] l_{so} shown here is obtained by averaging the extracted parameters below 4.5 K which are normally T-independent.

close to the MR peak occurring accompanied by the appearance of superconductivity in the 3-nm-thick film having faster spin relaxation. For the 12-nm-thick film, since superconducting correlation is rather strong and spin relaxation is comparably slower, MR peak is completely suppressed at low T. Different behavior in the films of different thicknesses results from different strength of spin relaxation and superconductivity. Spin-orbit coupling, which makes the spin degree of freedom respond to its orbital characteristics and causes spin relaxation, has thereby been demonstrated to have important effects on superconductivity. Our experimental work sheds new light on the understanding of the role of SO coupling in a superconductor.

Methods

All samples were grown *in situ* using a Varian Gen II solid-source molecular beam epitaxy (MBE) system. For an Al film whose thickness is 30–100 nm, an undoped 200-nm-thick GaAs buffer layers is grown on semi-insulating (100) GaAs substrate as a template. We find that the thickness of the GaAs buffer layer needs to be increased to 300 nm to achieve a flat enough template for depositing an aluminum nanofilm which is thinner than 15 nm. Before Al deposition, the buffer layer on top of the semi-insulating (100) GaAs substrate is kept in the ultra-high vacuum to prevent the GaAs surface from oxidation. After the growth chamber is pumped down to 3×10^{-10} Torr to eliminate residual arsenic vapor pressure, an Al nanofilm is grown at $\sim 0^{\circ}$C at a slow rate of 0.18 μm/h (0.05 nm/s) (ref. 42). We note that once the film thickness is below 2 nm, the Al nanofilm does not conduct at room temperature, suggesting that an ultrathin Al film gets oxidized and become Al_2O_3 which appears to be an insulator. For an Al nanofilm whose as-grown thickness ≥ 3 nm, the top Al_2O_3 film serves as a protective layer so that the underneath Al nanofilm does not get oxidized during processing. All samples were processed into 50-μm-wide Hall bars using conventional photo-lithography and lift-off technique. The mesa is defined by 2% tetramethylammonium hydroxide (TMAH) etching for 20 seconds for pattern transferring from photoresist to aluminum film. It is found that such a slow etch rate is crucial for high-yield, manageable and reliable sample preparation. A 30 nm/300 nm Ti/Au layer is deposited using electron-gun evaporation as the contact electrodes. Four-terminal magneto-transport measurements were carried out using dc constant-current sources in a top-loading He^3 cryostat equipped with a superconducting magnet. Since the device was patterned into Hall bar geometry one can obtain both longitudinal and Hall resistances R_{xx} and R_{xy}. In Fig. 3(a), we know that the mean free path l_0 is larger than the thickness ($\sim$6 nm) of the film being measured, indicating that the nanofilm in the present study can be treated as a quasi-two-dimensional system. Hence we can define longitudinal and Hall resistivities ρ_{xx} and ρ_{xy} by $\rho_{xx} = R_{xx}w/l$ and $\rho_{xx} = R_{xy}$, where w is the width of the Hall bar and l is the distance between the two voltage probes used for the measurement of R_{xx}. The same results were obtained on 3-nm and 12-nm-thick films. Source-drain current I_{SD} on the order of 10 μA was injected to improve the signal-to-noise ratio. For $I_{SD} < 1$ μA, the weak peak structures were hardly observed. Although large current may cause heating effects, which increases the electron temperature, our main findings regarding the coupling of spin-orbit coupling and superconductivity would not be influenced since I_{SD} is not large enough to completely destroy the superconducting state.

1. Wolf, S. A. *et al.* Spintronics: A Spin-Based Electronics Vision for the Future. *Science* **294**, 1488–1495 (2001).
2. Žutić, I., Fabian, J. & Das Sarma, S. Spintronics: Fundamentals and applications. *Rev. Mod. Phys.* **76**, 323–410 (2004).
3. Bader, S. D. & Parkin, S. S. P. Spintronics. *Annu. Rev. Condens. Matter Phys.* **1**, 71–88 (2010).
4. Sinova, J. *et al.* Universal Intrinsic Spin Hall Effect. *Phys. Rev. Lett.* **92**, 126603 (2004).
5. Jungwirth, T., Wunderlich, J. & Olejnik, K. Spin Hall effect devices. *Nat. Mater.* **11**, 382–390 (2012).
6. Quay, C. H. L. *et al.* Observation of a one-dimensional spin-orbit gap in a quantum wire. *Nat. Phys.* **6**, 336–339 (2010).
7. Erlingsson, S. I., Egues, J. C. & Loss, D. Energy spectra for quantum wires and two-dimensional electron gases in magnetic fields with Rashba and Dresselhaus spin-orbit interactions. *Phys. Rev. B* **82**, 155456 (2010).
8. Zimmermann, B. *et al.* Anisotropy of Spin Relaxation in Metals. *Phys. Rev. Lett.* **109**, 236603 (2012).
9. Yang, H., Yang, S.-H., Takahashi, S., Maekawa, S. & Parkin, S. S. P. Extremely long quasiparticle spin lifetimes in superconducting aluminium using MgO tunnel spin injectors. *Nat. Mater.* **9**, 586–593 (2010).
10. Debray, P. *et al.* All-electric quantum point contact spin-polarizer. *Nat. Nanotechnol.* **4**, 759–764 (2009).
11. Zhang, H. *et al.* Topological insulators in Bi_2Se_3, Bi_2Te_3 and Sb_2Te_3 with a single Dirac cone on the surface. *Nat. Phys.* **5**, 438–442 (2009).
12. Mourik, V. *et al.* Signatures of Majorana Fermions in Hybrid Superconductor-Semiconductor Nanowire Devices. *Science* **336**, 1003–1007 (2012).
13. Caviglia, A. D. *et al.* Tunable Rashba Spin-Orbit Interaction at Oxide Interfaces. *Phys. Rev. Lett.* **104**, 126803 (2010).
14. Ben Shalom, M., Sachs, M., Rakhmilevitch, D., Palevski, A. & Dagan, Y. Tuning Spin-Orbit Coupling and Superconductivity at the $SrTiO_3/LaAlO_3$ Interface: A Magnetotransport Study. *Phys. Rev. Lett.* **104**, 126802 (2010).
15. Dikin, D. A. *et al.* Coexistence of Superconductivity and Ferromagnetism in Two Dimensions. *Phys. Rev. Lett.* **107**, 056802 (2011).
16. Michaeli, K., Potter, A. C. & Lee, P. A. Superconducting and Ferromagnetic Phases in $SrTiO_3/LaAlO_3$ Oxide Interface Structures: Possibility of Finite Momentum Pairing. *Phys. Rev. Lett.* **108**, 117003 (2012).
17. Jeffrey Gardner, H. *et al.* Enhancement of superconductivity by a parallel magnetic field in two-dimensional superconductors. *Nat. Phys.* **7**, 895–900 (2011).
18. Bardeen, J., Cooper, L. N. & Schrieffer, J. R. Theory of Superconductivity. *Phys. Rev.* **108**, 1175–1204 (1957).
19. Koga, T., Nitta, J., Akazaki, T. & Takayanagi, H. Rashba Spin-Orbit Coupling Probed by the Weak Antilocalization Analysis in InAlAs/InGaAs/InAlAs Quantum Wells as a Function of Quantum Well Asymmetry. *Phys. Rev. Lett.* **89**, 046801 (2002).
20. Kohda, M., Bergsten, T. & Nitta, J. Manipulating Spin–Orbit Interaction in Semiconductors. *J. Phys. Soc. Jpn.* **77**, 031008 (2008).
21. Guzenko, V. A., Schäpers, T. & Hardtdegen, H. Weak antilocalization in high mobility $Ga_xIn_{1-x}As$/InP two-dimensional electron gases with strong spin-orbit coupling. *Phys. Rev. B* **76**, 165301 (2007).
22. Miller, J. B. *et al.* Gate-Controlled Spin-Orbit Quantum Interference Effects in Lateral Transport. *Phys. Rev. Lett.* **90**, 076807 (2003).
23. Zhou, W. Z. *et al.* Weak antilocalization and beating pattern in high electron mobility $Al_xGa_{1-x}N$/GaN two-dimensional electron gas with strong Rashba spin-orbit coupling. *J. Appl. Phys.* **104**, 053703 (2008).
24. Eshkol, M., Eisenberg, E., Karpovski, M. & Palevski, A. Dephasing time in a two-dimensional electron Fermi liquid. *Phys. Rev. B* **73**, 115318 (2006).
25. Pramanik, S. *et al.* Observation of extremely long spin relaxation times in an organic nanowire spin valve. *Nat. Nanotechnol.* **2**, 216–219 (2007).
26. Hikami, S., Larkin, A. I. & Nagaoka, Y. Spin-Orbit Interaction and Magnetoresistance in the Two Dimensional Random System. *Prog. Theor. Phys.* **63**, 707–710 (1980).
27. Sambandamurthy, G., Engel, L. W., Johansson, A. & Shahar, D. Superconductivity-Related Insulating Behavior. *Phys. Rev. Lett.* **92**, 107005 (2004).
28. Sambandamurthy, G., Engel, L. W., Johansson, A., Peled, E. & Shahar, D. Experimental Evidence for a Collective Insulating State in Two-Dimensional Superconductors. *Phys. Rev. Lett.* **94**, 017003 (2005).
29. Baturina, T. I., Mironov, A. Y., Vinokur, V. M., Baklanov, M. R. & Strunk, C. Localized Superconductivity in the Quantum-Critical Region of the Disorder-Driven Superconductor-Insulator Transition in TiN Thin Films. *Phys. Rev. Lett.* **99**, 257003 (2007).
30. Nguyen, H. Q. *et al.* Observation of Giant Positive Magnetoresistance in a Cooper Pair Insulator. *Phys. Rev. Lett.* **103**, 157001 (2009).
31. Lin, Y.-H. & Goldman, A. M. Magnetic-Field-Tuned Quantum Phase Transition in the Insulating Regime of Ultrathin Amorphous Bi Films. *Phys. Rev. Lett.* **106**, 127003 (2011).
32. Sacepe, B. *et al.* Localization of preformed Cooper pairs in disordered superconductors. *Nat. Phys.* **7**, 239–244 (2011).
33. Lo, S.-T. *et al.* Controllable Disorder in a Hybrid Nanoelectronic System: Realization of a Superconducting Diode. *Sci. Rep.* **3**, 2274 (2013).
34. Dubi, Y., Meir, Y. & Avishai, Y. Theory of the magnetoresistance of disordered superconducting films. *Phys. Rev. B* **73**, 054509 (2006).
35. Dubi, Y., Meir, Y. & Avishai, Y. Nature of the superconductor-insulator transition in disordered superconductors. *Nature* **449**, 876–880 (2007).
36. Dubi, Y., Meir, Y. & Avishai, Y. Island formation in disordered superconducting thin films at finite magnetic fields. *Phys. Rev. B* **78**, 024502 (2008).
37. Tan, K. H. S. B., Parendo, K. A. & Goldman, A. M. Evidence of spatially inhomogeneous pairing on the insulating side of a disorder-tuned superconductor-insulator transition. *Phys. Rev. B* **78**, 014506 (2008).
38. Lin, J. J. & Bird, J. P. Recent experimental studies of electron dephasing in metal and semiconductor mesoscopic structures. *J. Phys.: Condens. Matter* **14**, R501–R596 (2002).
39. Weng, M. Q. & Wu, M. W. Spin dephasing in n-type GaAs quantum wells. *Phys. Rev. B* **68**, 075312 (2003).
40. Kohda, M. *et al.* Spin–orbit induced electronic spin separation in semiconductor nanostructures. *Nat. Commun.* **3**, 1082 (2012).
41. Iordanskii, S. V., Lyanda-Geller, Y. B. & Pikus, G. E. Weak localization in quantum wells with spin-orbit interaction. *JETP Lett.* **60**, 206–211 (1994).
42. Lin, S.-W. *et al.* Characterization of Single-Crystalline Aluminum Thin Film on (100) GaAs Substrate. *Jpn. J. Appl. Phys.* **52**, 045801 (2013).

Acknowledgments

This work was supported by the NSC, Taiwan and National Taiwan University (grant no: 103R7552-2). We would like to thank Mr. Jheng-Cyuan Lin for experimental help and Prof. Tse-Ming Chen for helpful discussions.

Author contributions

S.T.L., S.W.L. and Y.T.W. performed the measurements. S.W.L. and S.D.L. prepared the samples. S.T.L. and C.T.L. drafted the paper. S.D.L. and C.T.L. coordinated the project.

Additional information

Supplementary information accompanies this paper at http://www.nature.com/scientificreports

Competing financial interests: The authors declare no competing financial interests.

How to cite this article: Lo, S.-T., Lin, S.-W., Wang, Y.-T., Lin, S.-D. & Liang, C.-T. Spin-orbit-coupled superconductivity. *Sci. Rep.* **4**, 5438; DOI:10.1038/srep05438 (2014).